Shining (Infrared) Light on the Hofmeister Series: Driving Forces for Changes in the Water Vibrational Spectra in Alkali-Halide Salt Solutions

Ashley K. Borkowski and Ward H. Thompson[a)]
Department of Chemistry, University of Kansas, Lawrence, KS 66045, USA

The Hofmeister series is frequently used to rank ions based on their behavior as chaotropes ("structure-breakers"), which weaken the surrounding hydrogen-bond network, to kosmotropes ("structure-makers"), which enhance it. Here, we use fluctuation theory to investigate the energetic and entropic driving forces underlying the Hofmeister series for aqueous alkali-halide solutions. Specifically, we exploit the OH stretch infrared (IR) spectrum in isotopically dilute HOD/D_2O solutions as a probe of the effect of the salt on the water properties for different concentrations and choice of halide anion. Fluctuation theory is used to calculate the temperature derivative of these IR spectra, including decomposition of the derivative into different energetic contributions. These contributions are used to determine the thermodynamic driving forces in terms of effective internal energy and entropic contributions. This analysis implicates entropic contributions as the key factor in the Hofmeister series behavior of the OH stretch IR spectra, while the effective internal energy is nearly ion independent.

I. INTRODUCTION

The Hofmeister series was originally developed to rank ions on the basis of their effect on the solubility of proteins, *i.e*, salting in or out. Since that time, it has been considered in much more general contexts related to how different ions modify water structure and dynamics. Underlying many of this is the notion that the Hofmeister series ranks ions as either chaotropes that disrupt the surrounding hydrogen-bonding (H-bonding) network or kosmotropes that enhance the H-bonding network.[1–12] Indeed, many groups have studied the structure and dynamics of aqueous salt solutions using scattering,[4–6,13] spectroscopic,[3–7,14–30] and computational[4–6,10–13,30–33] techniques. In addition to structural properties, significant work has particularly focused on dynamical properties in salt solutions, such as the water self-diffusion coefficient,[4–6,11,12,34] water OH reorientational dynamics,[4–6,32] and solution viscosity.[11]

One important approach for probing the Hofmeister series, and specifically its origin in the modifications of water H-bonding, is through the infrared (IR) and Raman spectroscopy of the water OH stretch in the presence of electrolytes. The changes in the vibrational spectra can probe the effects of ions on H-bonding with both the dissolved anions and water molecules in the solution. Numerous IR[14,16,18,20–24] and Raman[3,7,15,17,19,25] experiments have been conducted to determine the OH (or OD) stretching frequency for alkali-halides dissolved in H_2O, D_2O, or their isotopically dilute versions (HOD/D_2O or HOD/H_2O). Infrared,[14,16,18,23] attenuated total reflectance infrared,[20,24] femtosecond IR pump-probe,[21,22] and Raman[3,7,15,17,19,25,35] spectroscopy have been utilized and the measurements all observe the same trend: The shift in the OH vibrational stretching frequency in alkali-halide solutions is directly correlated with the halide size and consistent with the Hofmeister series. These results serve as both a point of reference and a source of motivation for the present theoretical study.

The use of vibrational spectra as a measure of ion effects is predicated on the fact that the OH stretching frequency is a key measure of the instantaneous H-bonding strength (though, notably a different measure of the strength than the enthalpy, internal energy, or free energy required to break the H-bond). That is, both the IR and Raman OH stretching spectra of liquid water are broad, reflective of the wide range of H-bonding environments experienced by the water molecules.[3,36,37]

At the same time, the spectra reflect other factors that can complicate the interpretation. One of these is resonant vibrational coupling between OH groups in water that can broaden the IR and Raman spectra, even leading to an additional peak in the case of the latter,[37–39] resulting in spectra that are less clearly reflections of the distribution of individual H-bonding environments. To avoid this effect, many studies have used isotopically dilute solutions, *e.g.*, HOD in H_2O or HOD in D_2O, and we do the same in the current work. Other confounding factors are not so readily eliminated. This includes non-Condon effects in which the OH transition dipole moment that determines the intensity of the IR signal increases with the H-bond strength;[37,40] this means that the IR spectrum is not a map of the distribution of instantaneous IR frequencies, but is instead less sensitive to higher frequency, more weakly H-bonded OH groups. It also includes dynamical effects, which lead to some motional narrowing of the OH stretching lineshape.[37] Despite these caveats, the OH stretching vibrational spectra can be highly informative. Changes in the IR spectrum upon the addition of salts can illuminate the shifts in the OH stretching frequencies where dynamical and non-Condon effects have more modest effects.

In this paper, we report a detailed examination of the temperature, concentration, and anion dependence of simulated IR spectra of the OH stretch in aqueous alkali-halide solutions. We use the empirical mapping technique

[a)]Electronic mail: wthompson@ku.edu

developed by Skinner, Corcelli, and co-workers[36,37,41–43] to calculate the IR spectra from classical molecular dynamics (MD) simulations; isotopically dilute HOD/D_2O is considered to avoid complications due to resonant vibrational coupling between OH bonds that is present in H_2O. As noted above, the trends with the different halide anions in measured spectra follow the Hofmeister series. Namely, the OH stretching frequency red-shifts, relative to that in neat water, with the addition of fluoride, but blue-shifts are observed for all the other halides, with the magnitude of the blue-shift increasing moving down the periodic table, *i.e.*, with the size of the anion. The empirical mapping-based simulation approach used in this work is fully consistent with these results.

The focus of the present work is on the thermodynamic driving forces that determine the IR spectra of electrolyte solutions. *i.e.*, an analysis of the *origin* of these changes to the OH vibrational spectrum that can provide new insight into the effect of these anions on the water structure and dynamics. To accomplish this, we use the recently developed fluctuation theory for dynamics approach,[44–46] which gives the temperature derivative of any dynamical quantity,[45] including the vibrational spectrum,[46] from simulations at a single temperature. More importantly for the current objective, fluctuation theory also provides the contributions to the temperature derivative from the different motions and interactions present in the system, *e.g.*, kinetic energy and Lennard-Jones and Coulombic interactions, representing otherwise unavailable mechanistic insight. In particular, the total temperature derivative can be used to determine the effective internal energy and entropy as a function of OH vibrational frequency and the contributions to the derivative yield the energetic components of the internal energy. Thus, this approach provides key insight into not only *how* different ions affect the OH stretching spectrum, but *why*, *i.e.*, the underlying energetic and entropic driving forces. In this way it gives additional mechanistic origins for the chaotropic and kosmotropic behavior that determine the Hofmeister series.

II. THEORY

The OH stretching IR spectra are calculated using the empirical mapping approach that estimates the quantum mechanical vibrational frequency and transition dipole moments from information directly available in a classical MD simulation.[36,37,41–43] Specifically, each quantity is written in terms of an empirical correlation, *e.g.*, the transition frequency is obtained as $\omega_{01} = c_0 + c_1\mathcal{E} + c_2\mathcal{E}^2$.

Here $\mathcal{E}$ is the (classical MD) electric field component along the OH bond evaluated at the H atom position and c_0, c_1, and c_2 are constants obtained from an empirical correlation of $\mathcal{E}$ with density functional theory-based calculations of ω_{01} in water clusters embedded in a point charge environment. The constants used in this work for ω_{01} and the transition dipole moment, μ_{01}, are taken from Ref. 37 and are given in Table S3. Note that these maps use scaled charges for the sodium (0.81379) and halide (0.92017) ions in the calculation of the electric field;[42] full ion charges are used in the MD simulations.

The IR line shape can then be calculated from the Fourier transform,

$$I(\omega) = \frac{1}{2\pi}\int_{-\infty}^{\infty} e^{-i\omega t}\phi(t)\,dt \tag{1}$$

where $\phi(t)$ is the dipole-dipole response function,

$$\phi(t) = \left\langle \vec{\mu}_{01}(0)\cdot\vec{\mu}_{01}(t)e^{i\int_0^t \omega_{01}(\tau)\,d\tau}\right\rangle e^{-|t|/2T_1} \tag{2}$$

Noting, $\vec{\mu}_{01}(t) = \langle 1|\hat{\mu}|0\rangle = \mu_{01}(t)\vec{e}_{OH}(t)$ is the matrix element of the transition dipole moment vector for the OH bond at time t, $\omega_{01}(t)$ is the $0\rightarrow 1$ vibrational frequency at time t obtained through the empirical mapping technique, and T_1 is the $n = 1$ vibrational relaxation lifetime set to the experimental value of 700 fs.[47] The brackets $\langle ...\rangle$ indicate a thermal average.

We recently showed how the temperature derivative of the IR spectrum can be calculated from simulations at a single temperature.[46] The approach is that of fluctuation theory for dynamics,[45] a natural extension of the well-established fluctuation theory in statistical mechanics.[48,49] Briefly, one can note that the thermal average of this dipole-dipole response function is dependent on temperature in only two places: The Boltzmann weighting factor and the canonical partition function, Q.

Then the derivative of the dipole-dipole response function with respect to $\beta = 1/k_BT$ results in the following expression:[46]

$$\begin{aligned}\frac{d\phi(t)}{d\beta} &= -\left\langle \delta H(0)\,\vec{\mu}_{01}(0)\cdot\vec{\mu}_{01}(t)e^{i\int_0^t \omega_{01}(\tau)\,d\tau}\right\rangle \\ &\quad\times e^{-|t|/2T_1} \\ &= -\phi_H(t),\end{aligned} \tag{3}$$

where k_B is the Boltzmann constant. In other words, the temperature derivative of the response function is a new response function that differs only in a weighting by the fluctuation of the total energy at $t = 0$, $\delta H(0) = H(0) - \langle H(0)\rangle$. In the notation of Eq. 3, the temperature derivative of IR spectrum is then,

$$\frac{dI(\omega)}{d\beta} = -\frac{1}{2\pi}\int_{-\infty}^{\infty} e^{-i\omega t}\phi_H(t)\,dt, \tag{4}$$

i.e., the negative of the Fourier transform of this weighted response function, $\phi_H(t)$. Note that this derivative can be calculated from the same simulation as $I(\omega)$ itself and thus both the spectrum and temperature derivative can be obtained from a single temperature simulation.

An additional attraction of this approach is realized by dividing the fluctuations of the total energy, $\delta H(0)$, into contributions from different energetic components, for example,

$$\delta H(0) = \delta KE(0) + \delta V_{Coul}(0) + \delta V_{LJ}(0), \tag{5}$$

where KE is the kinetic energy and V_{Coul} and V_{LJ} are the Lennard-Jones and Coulombic potential energies, respectively. The β derivative of the spectrum, Eq. 4, can then be decomposed as,

$$\begin{aligned}\frac{dI(\omega)}{d\beta} = &-\frac{1}{2\pi}\int_{-\infty}^{\infty} e^{-i\omega t}\phi_{KE}(t)\,dt \\ &-\frac{1}{2\pi}\int_{-\infty}^{\infty} e^{-i\omega t}\phi_{V_{Coul}}(t)\,dt \\ &-\frac{1}{2\pi}\int_{-\infty}^{\infty} e^{-i\omega t}\phi_{V_{LJ}}(t)\,dt,\end{aligned} \tag{6}$$

where, for example, $\phi_{KE}(t)$ has the same form as $\phi_H(t)$ in Eq. 3, but with $\delta KE(0)$ replacing $\delta H(0)$. We note that this is only one of the (simpler) possible decompositions. For example, the Coulombic potential energy can itself be written in terms of components from water-water, water-cation, water-anion, cation-cation, anion-anion, and cation-anion interactions, and the same is true of the Lennard-Jones energy. The contributions from each of these has been calculated to provide further insight into the effects, both direct and indirection, of the ions on the water spectrum.

III. SIMULATION METHODS

All MD simulations were performed using the Large-Scale Atomic/Molecular Massively Parallel Simulator (LAMMPS).[50,51] Each simulation consisted of SPC/E water molecules,[52] and ion pairs using the Joung-Cheatham model.[53] The simulations are of H_2O, but in calculating the OH stretch frequency and transition dipole moment, each OH is modeled as an HOD molecule surrounded by D_2O molecules as in isotopically dilute HOD/D_2O; this eliminates any resonant vibrational coupling between OH groups in H_2O. The force field parameters for each ion are given in Table S1. A total of five electrolyte solutions were considered. The first four have Na^+ as the cation with the halides F^-, Cl^-, Br^-, or I^- as the anion. However, because NaF is not soluble at concentrations $\gtrsim 1$ mol/kg,[54] we have also considered results for KF, which can be compared to measurements and does not differ substantially by the change in cation (see the Supporting Information where NaF and KF results are directly compared).

In all simulations, the timestep was 1 fs, the SHAKE algorithm was used for the water molecules, and the electrostatics were calculated using the particle-particle particle-mesh Ewald summation with an accuracy parameter of 1×10^{-4}. Note that tail corrections are applied for the Lennard-Jones interactions; these are included in V_{LJ} in Eqs. 5 and 6 just as the long-range contributions to the Ewald sum are included in V_{Coul}. Each system was first equilibrated for 500 ps and then propagated for 10 ns in the NpT ensemble at 1 bar and 298.15 K, using a Nosé-Hoover barostat and thermostat with a pressure and temperature chain length of three. The damping parameters for the barostat and the thermostat were 1000 and 100 fs, respectively. This NpT stage was used to determine the average volume, which was then used in subsequent NVT ensemble simulations. The differences in average volume resulting from the constant pressure equilibration of each solution give rise to small deviations from the nominal 1, 3, and 5 M concentrations and the precise values are given in Table S2. However, in the remainder of the paper we will, for example, refer to the approximately 3 M solution as "3 M" for simplicity.

Based on the calculated equilibrium volume, ten constant volume and temperature simulations were run for a 1 ns equilibration at 400 K followed by a 1 ns equilibration at 298.15 K, and finally a 4 ns run at 298.15 K. A Nosé-Hoover thermostat with a chain length of three and a damping parameter of 2 ps was used for all three stages. During the final run, the configurations and momenta were written every 4 fs. Errors in computed quantities were obtained by block averaging using 10 blocks (each block representing a single 4 ns trajectory) and are reported as 95% confidence intervals using the Student's t-distribution.[55]

IV. RESULTS AND DISCUSSION

A. IR Spectrum

The simulated OH stretching IR spectra, $I(\omega)$, of neat HOD/D_2O and varying concentrations of alkali-halides in HOD/D_2O are shown in Fig. 1. Note that the peak maximum is normalized to 1 and this normalization condition is extended to all temperature derivatives presented below.

We first discuss the shift of the peak maxima in the IR spectra as a function of concentration for the different alkali-halide solutions. Note that NaF is poorly soluble[54] so measurements correspond to KF given that the effect of the cation on the spectra is small as shown in Figs. S1,S3-S6 and Tables S4-S6 in the Supporting Information. We observe consistent shifts as the concentration for each halide is increased, with a sign and magnitude that depends on the halide identity. Specifically, the IR spectrum red-shifts when fluoride is added but blue-shifts for the other three sodium-halides. In the case of F^-, the red-shift is relatively modest, while for the other solutions the magnitude of the blue-shift increases moving down the periodic table and thus with the size of the halide. These trends are plotted in Fig. 2 and are qualitatively consistent with measurements[14,16,20,21] that show the same qualitative trends; see Fig. S2 for comparison between Ref. 16 Fig. 2 and this work. Specifically, we obtain good quantitative agreement for concentrations ≤ 2 molal., but overestimate the blue-shifts for higher concentrations where the measured spectra exhibit a saturation effect that is absent in the simulation results.[16]

We also observe changes in the linewidth with the

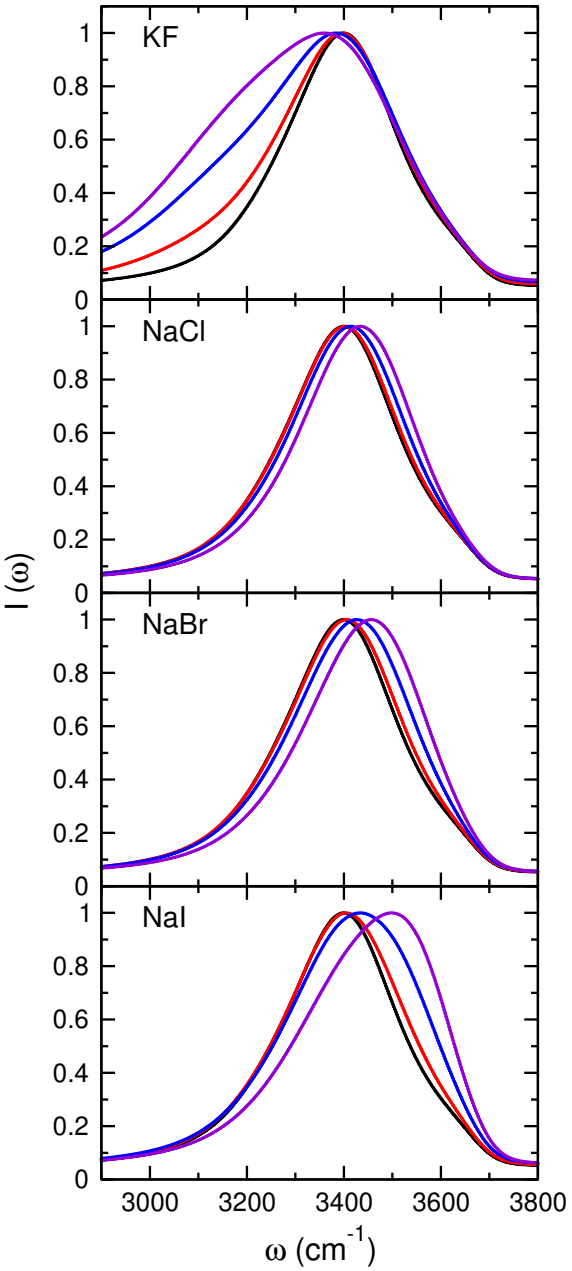

FIG. 1: HOD in D_2O IR spectra for neat water (black), 1 M (red), 3 M (blue), and 5 M (purple) of the four alkali-halides.

halide identity and concentration. The most dramatic effect is observed for KF, which broadens with increasing concentration. This is quantified by the full-width half-maximum (FWHM), which is plotted as a function of concentration in Fig. 2. The FWHM increases by ~ 170 cm^{-1} for 5 M KF compared to neat HOD/D_2O. In contrast, NaCl, NaBr, and NaI each show more modest broadening as the concentration is increased up to 3 M and then a slight narrowing from 3 to 5 M. The FWHM

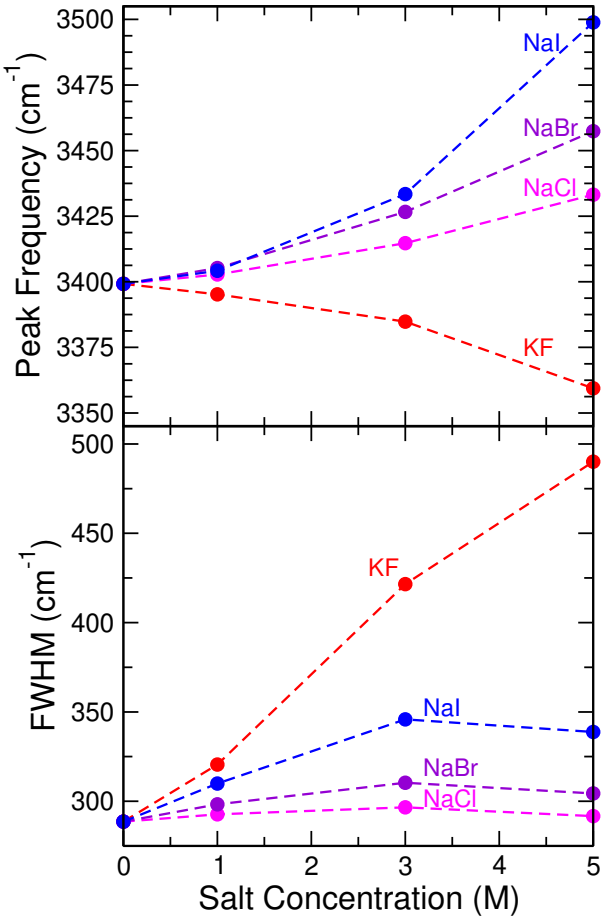

FIG. 2: Peak maxima (top) and full-width half-max (bottom) of the IR spectra of HOD in D_2O for KF (red), NaCl (magenta), NaBr (purple), and NaI (blue) as a function of concentration.

values are provided in Table S4.

B. Temperature Derivative of the IR Spectrum

We next focus on the derivatives of the IR spectrum with respect to β, evaluated using Eq. 4, to determine how the spectrum changes with temperature. Fig. 3 shows the total derivative, $dI(\omega)/d\beta$, for the OH stretching mode of HOD in D_2O for both the neat liquid and electrolyte solutions with varying salt concentrations. The general structure of the derivative is the same for all salts and concentrations. Namely, the derivative is positive at lower frequencies, peaking between 3350 and 3400 cm^{-1}, and negative at higher frequencies, reaching a minimum around $3550 - 3650$ cm^{-1}. Note that $dI(\omega)/dT = -(k_B T^2)^{-1}\, dI(\omega)/d\beta$ so that the positive peaks in the β derivative shown in Fig. 3 correspond to regions of the spectrum that will increase in magnitude as the temperature decreases. The results show that this

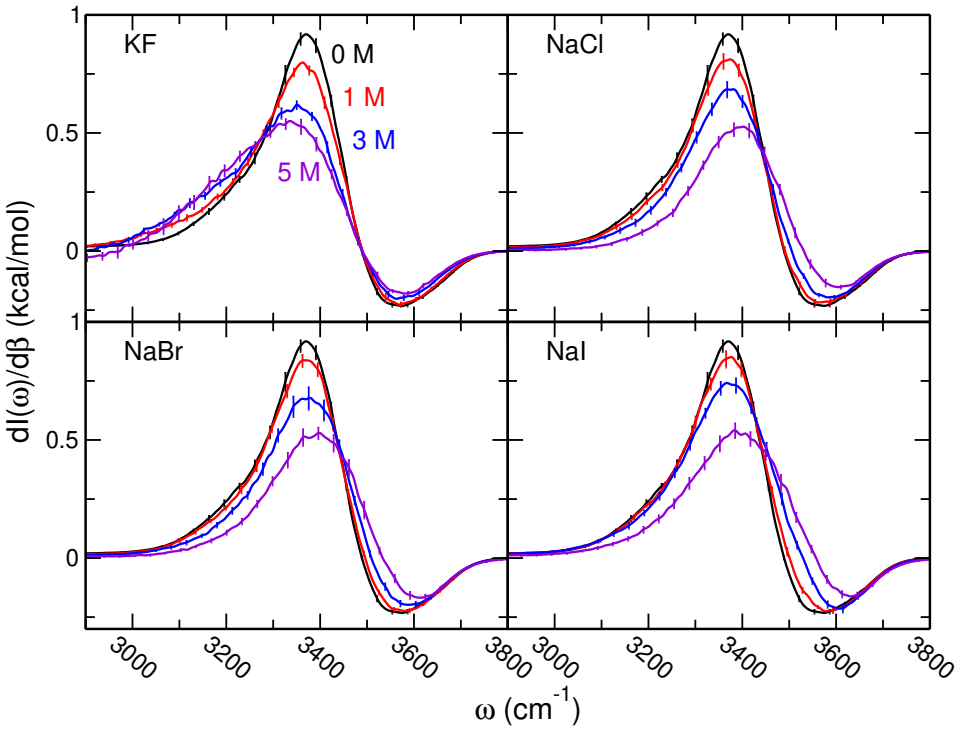

FIG. 3: Total derivative of the IR spectra with respect to β, obtained from Eq. 4, of HOD in D_2O for neat water (black), 1 M (red), 3 M (blue), and 5 M (purple) of the four alkali-halides.

corresponds to lower frequencies that are associated with OH groups engaged in stronger H-bonds (as measured by the transition frequency). Conversely, the negative region, which occurs at higher frequencies indicates that this part of the spectrum representing more weakly H-bonded OHs will increase in magnitude as T increases.

The height and location of the peak maximum and minimum of $dI(\omega)/d\beta$ both shift with increasing salt concentration. For all salts, the magnitude of the derivative, at both the maximum and minimum, decreases as the concentration increases, indicating that the addition of salt gives rise to a spectrum that is less sensitive to temperature, the driving forces for which are discussed below in Sec. IV D. In the case of KF, the position of the maximum in the derivative shifts to lower frequency with increasing concentration; the opposite is observed for the other halides with the frequency shift growing from Cl^- to Br^- to I^-. In a similar way, the location of the minimum value of the derivative is nearly independent of concentration for KF, but shifts to the blue for the other sodium halides. We will return to these trends below in the context of the underlying energetic driving forces.

These changes in the quantitative behavior of the derivative with frequency also affect the location of the isosbestic point, *i.e.*, the point at which $dI(\omega)/d\beta = 0$ and thus the spectrum is independent of T (at least over some range). It is important to note that this isosbestic point is not a consequence of two populations of water, but a natural result of the fact that the spectrum is related to an underlying frequency distribution (which must have a derivative with respect to temperature with both negative and positive values).[46,56] We find the isosbestic point of neat water at 3489.2 cm^{-1} (see Table S5), which lies between the results extra cted from the measurements of Kropman and Bakker[21] (3494 cm^{-1}) and Wyss and Falk[18] (3476 cm^{-1}). We find that the location of the isosbestic point is nearly independent of concentration for KF, but shifts to the blue for the sodium halides considered, by 40.6 cm^{-1} for NaCl, 37.3 cm^{-1} for NaBr, and 56.5 cm^{-1} for NaI.

C. Decomposition of the Temperature Derivative of the IR Spectrum

1. *Contributions by Interaction Type*

Temperature derivatives of vibrational spectra, such as those shown in Fig. 3, have been obtained experimentally by determining the numerical derivative from measurements at multiple temperatures.[57,58] However, more detailed determinations of the energetic driving forces underlying the temperature derivative is not possible from experiments. In contrast, because $dI(\omega)/d\beta$ is obtained as an analytical derivative as described in Sec. II, the contribution to the derivative from any component of the total energy of the system can be obtained. This provides key mechanistic insight that is not available in any other

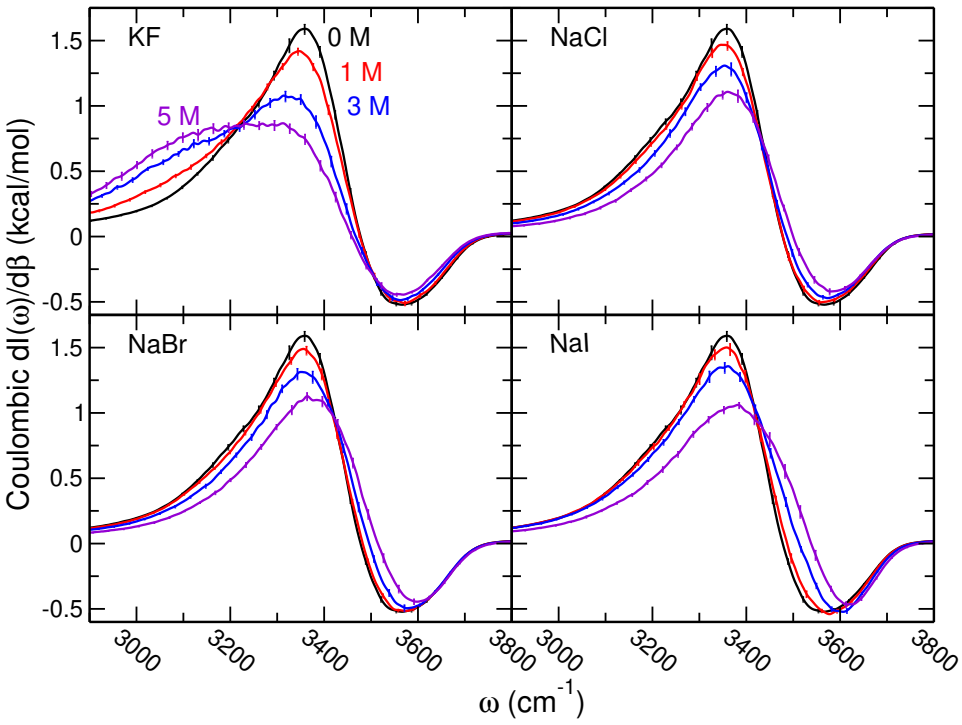

FIG. 4: Coulombic potential energy contribution to the total derivative of the IR spectrum with respect to β as given by Eqs. 5 and 6. Results are shown for HOD in D_2O for neat water (black) and 1 M (red), 3 M (blue), and 5 M (purple) solutions of the four alkali-halides.

way.

In the simplest approach of this kind, we divide the total energy into the kinetic energy and Coulombic and Lennard-Jones interactions and determine the contribution of each of these to the temperature derivative $dI(\omega)/d\beta$ as outlined in Eq. 6. Note that each derivative contribution illustrates how increasing that particular component of the energy changes the spectrum. To be precise, the Coulombic contribution to $dI(\omega)/d\beta$, for example, indicates how reducing the Coulombic potential energy would shift the spectrum; this notes that the derivative is with respect to β not T and represents how the change in Coulombic energy with T affects the spectrum, separate from the change in other energy components.

We first note that, compared to the Coulombic and Lennard-Jones potential energy contributions, the kinetic energy component of the derivative is quite small and mirrors the qualitative shape of the total $dI(\omega)/d\beta$.[46] Thus, we do not focus on these results, which are shown in Fig. S5. We do note that this implies only a minor dynamical effect on the changes in the IR spectrum with temperature.

The Coulombic potential energy contributions to the β derivative of the IR spectra are shown in Fig. 4. The contribution fairly closely resembles that of the total derivative shown in Fig. 3, but with a larger magnitude (note the different scales on the vertical axes). In particular, the Coulombic energy contribution favors lower (higher) frequencies at T is reduced (increased), as the total derivative does. The trends with salt concentration are also qualitatively the same as for the total derivative. Thus, we can see that the Coulombic contribution is, unsurprisingly, the dominant one and its features are largely retained in the total $dI(\omega)/d\beta$. The quantitative differences are illustrated in the positions of the isosbestic points, *i.e.*, the frequency at which $dI(\omega)/d\beta = 0$. For the Coulombic contribution, the isosbestic frequency trends with the anion identity are clearer and more consistent: Increasing the concentration from 1 to 5 M leads to a shift in the isosbestic point of -17.3, 12.7, 32.1, and 51.1 cm^{-1} for KF, NaCl, NaBr, and NaI, respectively (see Table S5).

The Lennard-Jones potential energy contributions to the total IR spectra β derivatives are presented in Fig. 5 and differ notably from the Coulombic contributions. Of particular note is that the derivative contribution is negative at lower frequencies and positive at higher frequencies. This indicates that lowering the Lennard-Jones energy by reducing T (increasing β) tends to blue-shift the spectrum, favoring higher frequency, more weakly H-bonded arrangements of the OH groups and disfavoring the stronger, more red-shifted H-bonds. This shows a clear competition between the Coulombic interactions, which favors stronger H-bonds, and is consistent with our previous simulations of neat water[46] as well as wa-

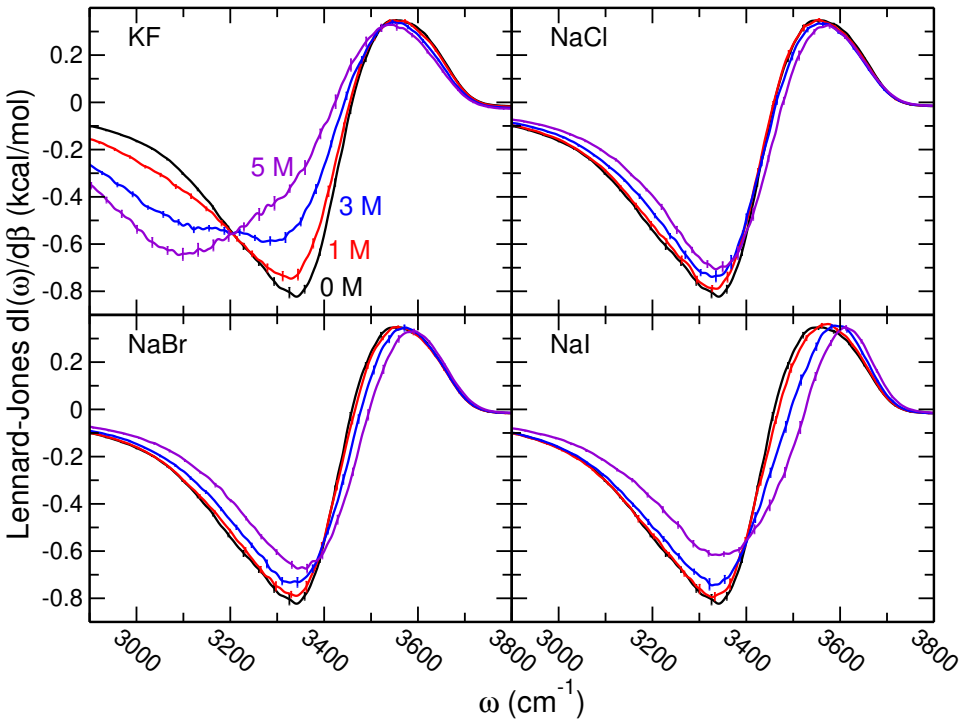

FIG. 5: Same as Fig. 4 but the Lennard-Jones potential energy contribution to $dI(\omega)/d\beta$ is shown as given by Eqs. 5 and 6.

ter diffusion,[12,59–61] reorientation,[59–63] viscosity,[64] and H-bond exchange dynamics.[61,63] The Coulombic contributions, as noted above, dominate, which is clear from the relative magnitude of the two contributions; note the difference in vertical axis scale between Figs. 4 and 5. The Lennard-Jones contribution to the derivative is also sensitive to the salt concentration. Once again, this can be illustrated by the position of the isosbestic point, which shifts by −31.5, 19.6, 30.8, and 57.2 cm^{-1} for for KF, NaCl, NaBr, and NaI, respectively, as the salt concentration is increased from 1 to 5 M (see Table S5). The location of the (measurable) isosbestic points for each salt solution is determined by the competition between the dominant electrostatic interactions and these opposing Lennard-Jones interactions.

2. *Contributions by Molecular Interactions*

A more detailed mechanistic picture of the factors determining how temperature affects the IR spectrum is obtained by examining the contributions from interactions between the different species – *i.e.*, water, anions, and cations – present in the salt solutions. Specifically, we have calculated the contribution to $dI(\omega)/d\beta$ associated with the water-water, water-cation, water-anion, cation-cation, anion-anion, and cation-anion interactions. In each case, we have separately computed the Coulombic and Lennard-Jones contributions, giving twelve total components of the derivative (excluding the kinetic energy terms that, as noted above, have a small effect). We note that, as will be shown below, the magnitude of these contributions to the derivative are directly related to their effect on the effective internal energy of the IR spectrum as a function of frequency. In this way, the decomposition presented here provides insight into the driving forces that shape the IR spectra.

These contributions to the β derivative of the IR spectrum are shown in Fig. 6 for NaCl at 1, 3, and 5 M concentrations. At the lowest, 1 M, concentration, the derivative is dominated by the water–water interactions, which nearly equal the total for both the Coulombic and Lennard-Jones contributions. The only other non-negligible Coulombic contributions come from the water–Na^+ and water–Cl^- and Na^+–Cl^- interactions. The former two favor stronger H-bonding arrangements, *i.e.*, they peak at lower frequencies which are thus favored by these interactions as T decreases, and are opposed by the cation-anion interactions. In the Lennard-Jones contributions, the water–Cl^- interactions are the only other non-negligible contribution and they favor weaker H-bonding structures; given their short-range nature, these must correspond to the direct water–Cl^- H-bonding.

As concentration is increased, the Lennard-Jones contributions to the derivative shrink in magnitude, primarily due to the water–water interactions. As more salt is added, the contribution from water–Cl^- interactions grows and a small contribution from Na^+–Cl^- interac-

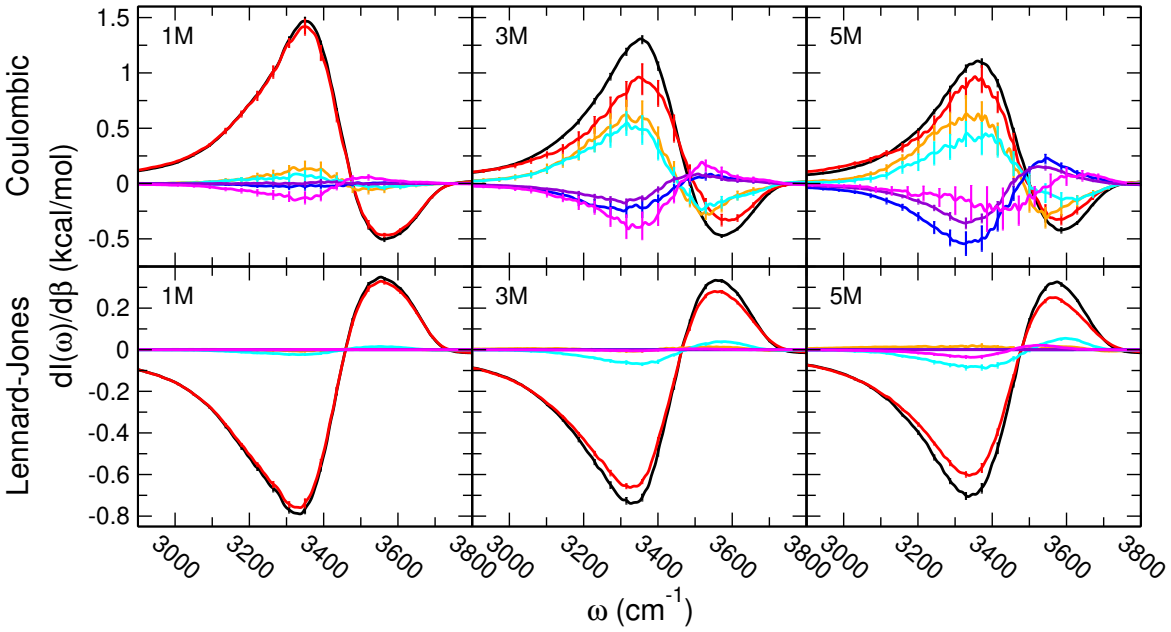

FIG. 6: Contributions to the β derivative of the IR spectrum due to Coulombic (top) and Lennard-Jones (bottom) potential energy interactions of 1, 3, and 5 M NaCl in HOD/D_2O. Results are shown for the contributions due to the potential energy associated with all (black), water-water (red), water-sodium (orange), water-chloride (cyan), sodium-sodium (blue), chloride-chloride (purple), and sodium-chloride (magenta) interactions.

tions is observed at 5 M, presumably due to the presence of contact-ion pairs at that high concentration. All other Lennard-Jones interactions have a negligible effect on $\partial I(\omega)/\partial\beta$.

The picture is more complicated for the Coulombic contributions to the derivative. As the concentration increases, the overall derivative decreases in magnitude due to a reduction in the water–water contributions to $\partial I(\omega)/\partial\beta$ and the rise of several competing contributions associated with the ions. Specifically, the water–Na^+ and water–Cl^- interactions grow in magnitude sharply as the salt concentration increases from 1 to 3 M, but only change modestly from 3 to 5 M. They are the only interactions involving ions that favor lower frequency, stronger H-bonded OHs. Interestingly, the water–Na^+ contribution is the larger of the two. As the concentration increases, the Na^+–Na^+, and Cl^-–Cl^- interaction components grow steadily in magnitude and acting in opposition to the water–ion contributions. The Na^+–Cl^- contribution first grows as the NaCl concentration is increased to 3 M and then decreases and shifts to the blue as it is further raised to 5 M. The results suggest an interesting interplay between the interactions present in these salt solutions, which reshuffles as the concentration is increased such that a larger fraction of waters are immediately adjacent to an ion and ions are in closer proximity to each other.

It is also interesting to examine how the various interactions contribute for different salts. This is examined in Fig. 7 where the Coulombic and Lennard-Jones contributions of the different potential energy terms are shown for 3 M solutions of KF, NaCl, NaBr, and NaI.

Focusing first on the Lennard-Jones components, we can see that the only meaningful contributions at 3 M come from the water–water and water–halide interactions. Clear trends are observed in that the total Lennard-Jones contribution to the derivative and the dominant water–water term increase moving down the halide series, *i.e.*, with increasing halide size. The water–halide Lennard-Jones contribution, on the other hand, decreases with the halide size so that it is nearly negligible for NaI. We have previously shown that the Lennard-Jones interactions favor weaker H-bonds because strong H-bonds, held together by Coulombic interactions, sit on the repulsive wall of the Lennard-Jones potential between the the donating water molecule and the H-bond acceptor. Thus, the Lennard-Jones results in Fig. 7 indicate that the more charge-dense halides that form stronger H-bonds do so at the expense of favorable Lennard-Jones interactions, *i.e.*, those H-bonds sit even further up on the Lennard-Jones repulsive wall.

Again, the situation is more complex for the Coulombic contributions where every interaction type makes a non-negligible contribution. In all cases, the water–water interactions represent the largest component. The water–water terms is nearly identical for the three sodium-halide solutions considered, but differs for the KF case by the appearance of a significant shoulder at lower frequency, centered around 3100 cm^{-1}. The water–Na^+ contribution is the next largest for the sodium-halide

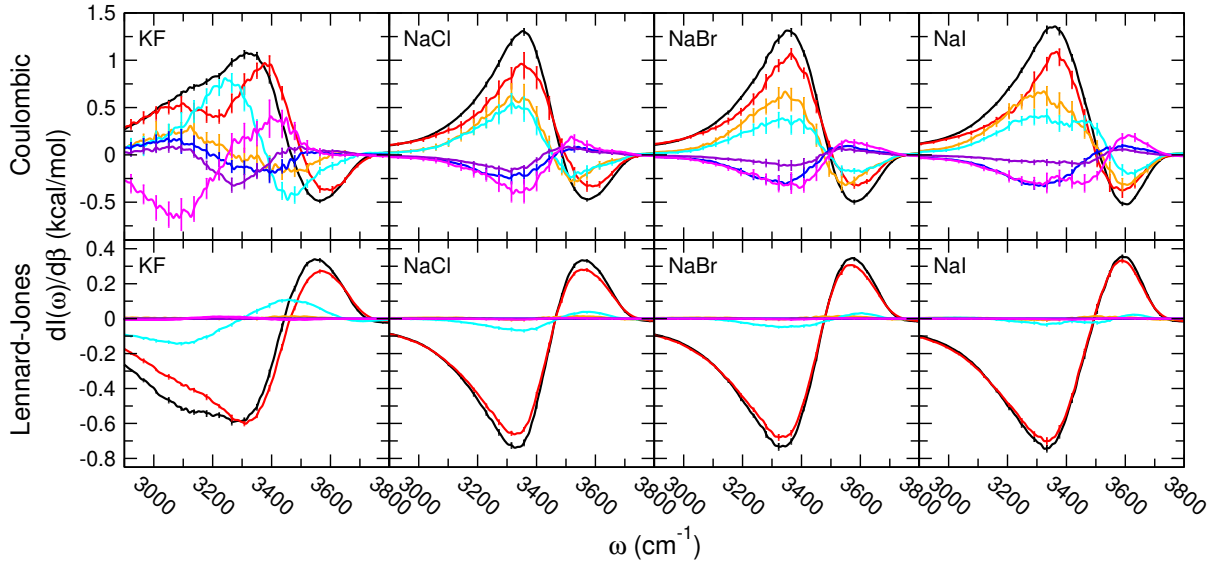

FIG. 7: Same as Fig. 6 except that results are shown for 3 M solutions of KF, NaCl, NaBr, and NaI in HOD/D_2O. Results are shown for the contributions due to the potential energy associated with all (black), water-water (red), water-alkali (orange), water-halide (cyan), alkali-alkali (blue), halide-halide (purple), and alkali-halide (magenta) interactions.

solutions and depends only weakly on the halide, with a slight blue-shifting of the derivative contribution observed with increasing halide size. The water–K^+ contribution for KF is comparatively smaller and strongly red-shifted. The water–halide interactions also contribute strongly with a modest halide dependence manifested as a reduction in the magnitude and a blue-shift of the derivative contribution moving down the halide series.

The fact that the water–Na^+ contribution to the β derivative of the IR spectrum is larger than the water-anion one is surprising result, given the direct effect water-halide H-bonding has on the vibrational frequencies of the OH groups involved. However, we note that the data suggest these effects may be associated with the overall influence of the ions on the solution behavior rather than direct ion-OH group interactions. Specifically, the cation-water Lennard-Jones contribution to the derivative, which is short-ranged and thus most prominent for direct water-ion interactions, is essentially negligible, while the anion-water Lennard-Jones contribution is significant, but considerably smaller than the corresponding Coulombic component. It should be possible in the future, with greater statistical sampling, to distinguish the effect of the cations and anions on the IR spectrum for OH groups in their first solvation shell, as we have done previously in the case of diffusion.[12]

The ion–ion contributions to $\partial I(\omega)/\partial\beta$ are comparatively smaller for the sodium-halide solutions. The largest of these contributions comes from the Na^+-halide interactions and favors weaker H-bonding arrangements; its magnitude does not change with the halide but shifts to higher frequencies as the halide size increases. The K^+–F^- component is significantly larger in comparison and shifted strongly to lower frequencies; this can be attributed to the strong coordination of the fluoride ion, as little difference is observed for the NaF case as shown in Fig. S6. The Na^+–Na^+ and halide-halide interactions are the smallest contributions for the sodium-halide solutions. The former is nearly independent of halide identity while the latter decreases in magnitude and shifts to the blue with increasing halide size. For the KF solution, the K^+–K^+ contribution to the derivative favors lower frequencies, stronger H-bonding in contrast to the sodium-halide solutions. The F^-–F^- contribution to the derivative is positive at both higher and lower frequencies and negative around 3300 cm^{-1}. Clearly, the compact charge density of fluoride, which makes it an exceptionally strong H-bond acceptor as well as a strong coordination partner with the cation, leads to qualitative changes from the behavior observed for the other halides.

D. Thermodynamic Driving Forces

The temperature derivatives presented above can be used to obtain more direct, intuitive measures of the thermodynamic driving forces for the vibrational spectra. In particular, we can use them, with the spectra, to address the relative role of energetic and entropic effects. Although it is not possible to rigorously calculate an internal energy or entropy from an IR spectrum because it is a dynamical quantity, one can define an *effective* internal energy, $\Delta U_{IR}(\omega)$, and effective entropy, $\Delta S_{IR}(\omega)$, as

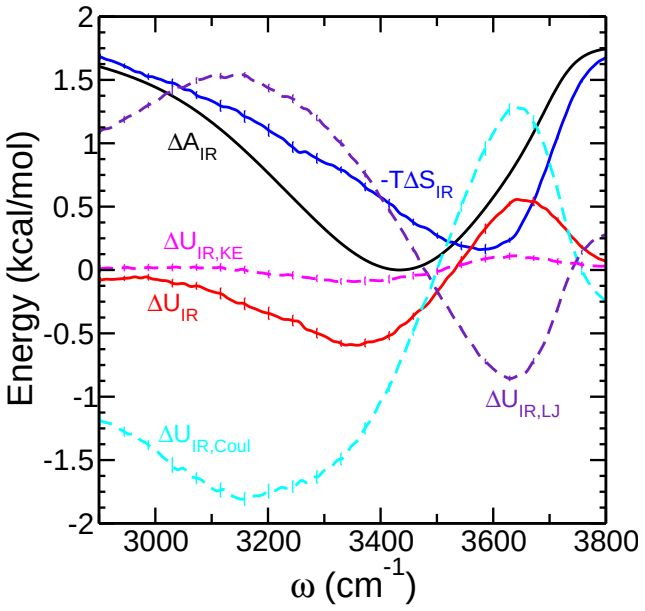

FIG. 8: Effective Helmholtz free energy ΔA_{IR} (black), effective internal energy ΔU_{IR} (red), and effective entropic contribution $-T\Delta S_{IR}$ (blue) are shown along with the kinetic (dashed magenta), Lennard-Jones (dashed purple), and Coulombic (dashed cyan) effective internal energy components for the IR spectrum of HOD in D_2O for 5 M NaCl.

a function of frequency as

$$\Delta U_{IR}(\omega) = -\left(\frac{\partial \ln I(\omega)}{\partial \beta}\right) \tag{7}$$

and

$$\Delta S_{IR}(\omega) = \frac{\Delta U_{IR}(\omega) - \Delta A_{IR}(\omega)}{T}. \tag{8}$$

Here, the effective Helmholtz free energy associated with the IR spectrum as a function of frequency is

$$\begin{aligned} \Delta A_{IR}(\omega) &= -k_B T \ln I(\omega) \\ &= \Delta U_{IR}(\omega) - T\Delta S_{IR}(\omega). \end{aligned} \tag{9}$$

Such approaches have previously been used for both Raman[57,58] and IR spectra[46] and provide the most direct insight into the thermodynamic driving forces determining both the spectrum and its temperature dependence (*vide infra*). It is important to note, however, that despite previous interpretations,[57,58] these thermodynamic profiles do not provide information about the energy (or entropy) required to break an H-bond. Rather, they represent the changes in energy or entropy associated with changing the OH frequency, which does *not* require the scission of the H-bond.[46]

These energy profiles are shown for 5 M NaCl in Fig. 8, where the internal energy is also further decomposed, using Eq. 6, into contributions from the Coulombic and Lennard-Jones interactions and kinetic energy. The essential features observed for this case are common across all the solutions considered here. Namely, the internal energy has a minimum below 3400 cm^{-1} while the entropic contribution is lowest near 3600 cm^{-1}; both rise more sharply to higher frequencies (corresponding to more weakly H-bonded OHs) and more slowly to red-shifted frequencies (corresponding to more strongly H-bonded OHs). The opposition of the energetic and entropic effects leads to a minimum in the effective free energy (peak maximum in the IR spectrum) at an intermediate frequency, in this case near 3440 cm^{-1}. The internal energy is dominated by the contribution from Coulombic interactions, which is opposed by the Lennard-Jones component while the kinetic energy contribution is quite small.

A key benefit of this analysis within fluctuation theory for dynamics is that it enables an examination of the relative influence of (internal) energy and entropy on the spectral changes observed upon the addition of salt. The effective Helmholtz free energy, $\Delta A_{IR}(\omega)$, is shown in Fig. 9 for both neat HOD/D_2O and varying concentrations of salts in HOD/D_2O. Because $\Delta A_{IR}(\omega)$ is a simple function of the IR spectrum, it mirrors the behavior observed in the spectra that is discussed above. For example, the free energy minima are found at the frequencies corresponding to the IR peak maxima (see Tables S4 and S6). However, the frequency at which the free energy reaches a minimum and the shape the free energy profile are determined by the combination of the internal energy and entropy, Eq. 9, and we now examine those factors to understand their relative influence.

The effective internal energy, $\Delta U_{IR}(\omega)$, given by Eq. 7 is also shown in Fig. 9 for neat water and the salt solutions at 1, 3, and 5 M. Note that we have set the minimum for each curve at zero to more clearly illustrate any differences in the frequency dependence of the internal energy. As noted above, the internal energy profile has the same qualitative shape for all the solutions considered. Of particular note is that, for NaCl, NaBr, and NaI, the global minimum of the internal energy profile appears at a frequency that is nearly independent of the identity of the halide anion and the concentration. Indeed, the internal energy profiles for these three salts at a given concentration are nearly identical (except around the peak at high frequencies). More specifically, this says that the internal energy required to change an OH from the lowest energy frequency at $\sim$ 3350 cm^{-1} to a lower frequency, more strongly H-bonded arrangement or a higher frequency, more weakly H-bonded structure is independent of the halide ion. In other words, the internal energy does not exhibit a Hofmeister effect for these three halides.

Two small differences in $\Delta U_{IR}(\omega)$ are observed for KF compared to these three salts. First, the location of the energy minimum is shifted to lower frequencies for the 3 and 5 M solutions. Second, at these higher concentrations there a smaller increase in internal energy required to move from the lowest energy frequency to stronger

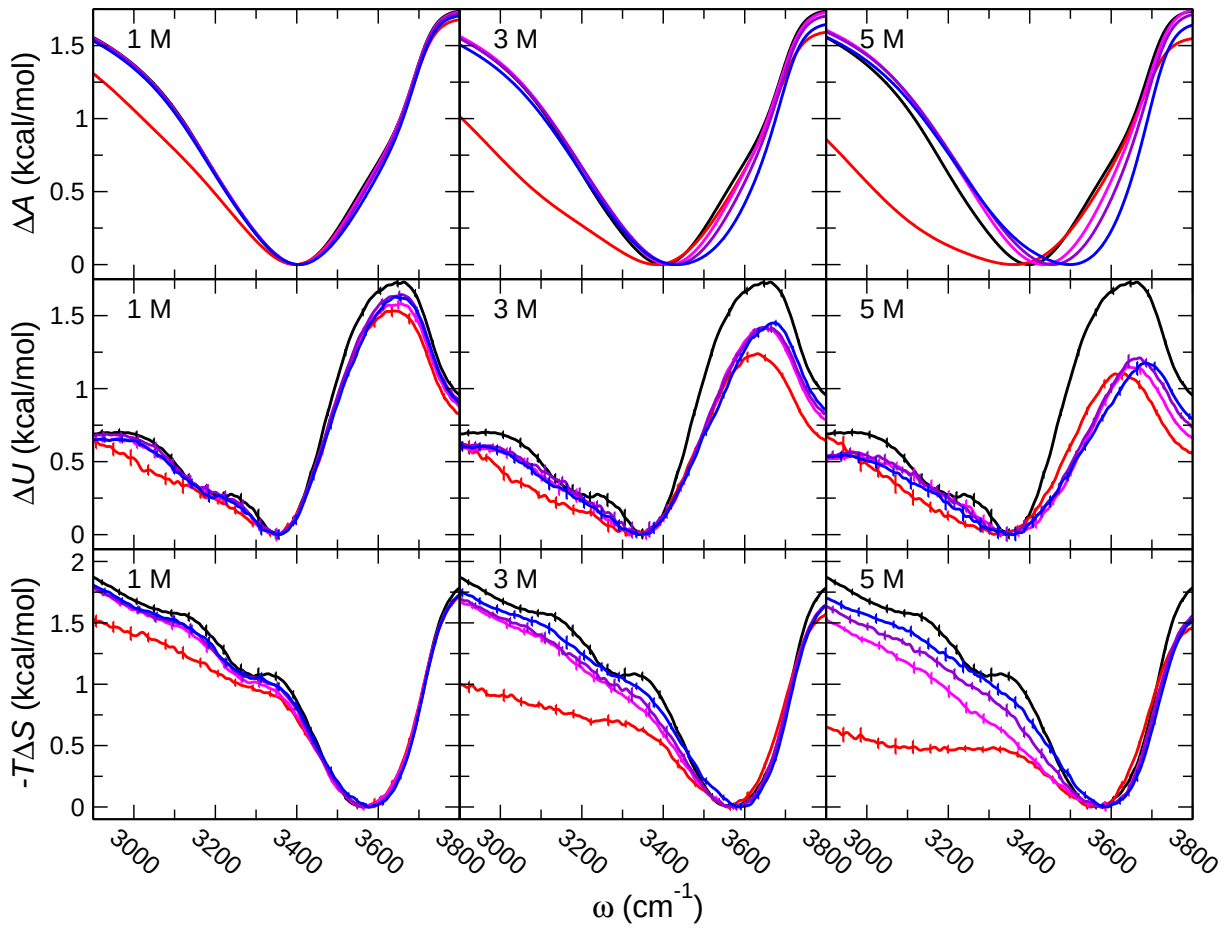

FIG. 9: Effective Helmholtz free energy ΔA_{IR} (top row), effective internal energy ΔU_{IR} (middle row), and effective entropic contrition $-T\Delta S_{IR}$ (bottom row) of the IR spectra of HOD in D_2O for neat water (black), KF (red), NaCl (magenta), NaBr (purple) and NaI (blue) at 1 M (left), 3 M (middle), and 5 M (right). In each panel, the minimum value of each curve is set to zero.

or weaker H-bonded arrangements (lower or higher vibrational frequencies, respectively). In these ways, the internal energy shows a modest Hofmeister effect for KF relative to the other halides.

It can also be seen that the 1 M salt solutions have $\Delta U_{IR}(\omega)$ that are only slightly changed from the neat HOD in D_2O case. As the concentration is increased to 3 and then 5 M, the internal energy profile becomes flatter, *i.e.*, the internal energy changes with OH frequency are reduced. Insight into the origins of this behavior can be gleaned from inspection of Fig. 6. Those data indicate that the Lennard-Jones contribution to the derivative, and hence $\Delta U_{IR}(\omega)$, changes little with concentration such that changes in the Coulombic interactions are the primary cause of the flattening of the internal energy profile with salt concentration. More specifically, we see two trends that lead to less variation in ΔU_{IR} with ω: 1) As the concentration increases, ion-water interactions replace water-water interactions and the former tend to have a lower internal energy for high frequency, weak H-bonds compared to the latter. 2) The ion-ion interactions act to oppose the internal energy of the water-water and water-ion interactions, *i.e.*, they lower (raise) the internal energy of higher (lower) frequency H-bonds. However, it is important to note that this flattening of the $\Delta U_{IR}(\omega)$ profile with increasing salt concentration cannot explain the changes in the FWHM of the IR spectra of the sodium-halides considered, Fig. 2, which increase from 1 to 3 M and then decrease or stay the same when the concentration is raised to 5 M.

Finally, the effective entropic contribution, $-T\Delta S_{IR}(\omega)$, calculated from Eq. 8 is also shown in Fig. 9 for neat water (HOD in D_2O) and the salt solutions. Note that all minima are set to zero in order to investigate the effective entropy as a function of halide and concentration. As with $\Delta U_{IR}(\omega)$, the entropic contribution shows different behavior for KF compared to the other sodium-halide solutions. But unlike for the internal energy, $-T\Delta S_{IR}(\omega)$ shows a clear trend for the series of halides with increasing salt

concentration. In particular, the entropic cost associated with strengthening of the H-bond, *i.e.*, moving to lower vibrational frequencies, depends increasingly on the halide at higher concentrations. Namely, with increasing concentration entropy lowers the free energy associated with stronger H-bonds with more red-shifted vibrational frequencies. However, the effect is slight for NaI and increases moving down the halide series with the largest effect for KF. This is the origin of the Hofmeister effect observed in the IR spectrum itself, which is red-shifted for KF and blue-shifted increasingly for the other halides in the order NaCl, NaBr, and NaI.

Overall, the manifestation of the Hofmeister effect in the frequency shifts in the IR spectrum are a consequence of two factors: 1) The flattening of the internal energy profile with growing salt concentration, which serves to increase the weight of the entropic contribution, and 2) The reduction in the entropic penalty for forming stronger H-bonds that is more prominent the smaller the halide. The former is nearly independent of the halide identity, while the latter depends significantly on it. Overall, while both internal energy and entropy determine the frequency shift with addition of salt, this clearly implicates entropic contributions as the central driving force for the Hofmeister trend in the IR spectra.

It is perhaps counterintuitive that lower water OH vibrational frequencies in salt solutions are favored entropically rather than energetically. While further, even more detailed, studies are necessary to fully explore these factors, it is useful to note some relevant caveats. First, we note that none of the present results are for the infinitely dilute case or restricted to the first solvation shell of a halide. Thus both the internal energy and entropy reflect the overall electrolyte environment. For example, the entropic profiles in Fig. 9 indicate that increasing the salt concentration results in more arrangements for an OH group to have a lower frequency and this effect grows inversely with the halide size. At the same time, the internal energy for an OH to have a lower frequency is nearly independent of halide size. We cannot yet say whether this is a reflection of the entropy and internal energy as a function of frequency for an individual water OH interacting with a particular halide, a point that requires a different approach than that used here.

E. Predicting IR Spectrum at Different Temperatures

Knowledge of the effective internal energy profile as a function of frequency, $\Delta U_{IR}(\omega)$, enables the prediction of the IR spectra as a function of temperature using only the present room temperature simulations. We have previously shown that a van't Hoff approximation,

$$I_{pred}(\omega;T_b) = \frac{I(\omega;T_a)\, e^{-(\beta_b-\beta_a)\Delta U_{IR}(\omega)}}{\int_0^\infty P(\omega;T_a)\, e^{-(\beta_b-\beta_a)\Delta U(\omega)d\omega}}, \qquad (10)$$

can accurately predict the IR spectrum of HOD in D_2O over a temperature range of $280-370$ K.[46] Here, $\beta_a = 1/k_BT_a$, $\beta_b = 1/k_BT_b$, $P(\omega;T)$ is the vibrational frequency distribution at temperature T, and $\Delta U(\omega)$ is the effective internal energy associated with the frequency distribution. The denominator in Eq. 10 accounts for the fact that the van't Hoff factor, $e^{-(\beta_b-\beta_a)\Delta U_{IR}(\omega)}$ is not norm-conserving.

The predicted IR spectra for the OH stretch in isotopically dilute NaCl solutions are shown in Fig. 10 for temperatures from 280 to 370 K. At all salt concentrations, the spectrum blue-shifts to higher frequencies and the overall intensity decreases as the temperature is increased. These effects, however, decrease within increasing NaCl concentration so that the temperature effects are significantly more modest in the 5 M solution compared to neat water and 1 M NaCl.

Measurements by Wyss and Falk of the IR spectra of neat HOD/D_2O and ~ 5 M NaCl solutions found similar behavior. As the temperature is increased, they observed that the peak frequency increases and the peak absorptivity decreases for both neat water and the NaCl solution.[18] Specifically, upon increasing the temperature from 283 to 358 K they observed a blue-shift in the peak frequency of ~ 50 cm^{-1} for HOD in D_2O compared to 25 cm^{-1} in the NaCl solution, where we find shifts of 38.7 cm^{-1} and 24.4 cm^{-1}, respectively, for these two systems between 280 and 360 K. Similar results were found by Masuda and co-workers in ATR-IR spectroscopy measurements on neat water and solutions with increasing concentrations of NaCl.[20]

Kropman and Bakker examined the temperature dependence of the IR spectra of neat HOD in D_2O and 6 M NaI in HOD in D_2O as part of a study of salt effects on vibrational relaxation.[21] They found that the OH stretching peak blue-shifts by ~ 50 cm^{-1} in HOD in D_2O between 298 and 366 K. This is in good agreement with the results of Wyss and Falk[18] and somewhat larger than our prediction of 34.6 cm^{-1} upon heating from 298 to 370 K. In contrast, the peak blue-shifts by only 10 cm^{-1} in the NaI solution over the same temperature range. In the present simulations, we find a blue-shift of 22.4 cm^{-1} for 5 M NaI from 298 to 370 K. They also observe a more modest reduction of the peak intensity in the NaI solution compared to neat water, consistent with the present results (see Fig. S7).

Thus, the present results (based on the Joung-Cheatham[53] and SPC/E[52] models for the ions and water) semi-quantitatively predict the results from measurements of the IR spectra. We note that our previous simulations of neat HOD in D_2O using the TIP4P/2005 water model[65] gave a blue-shift of ~ 47 cm^{-1} when the temperature is raised from 298 to 360 K, in better agreement with the measured data.

V. CONCLUSIONS

We have presented the results of MD simulations of the OH stretching IR spectra of KF, NaCl, NaBr, and NaI in

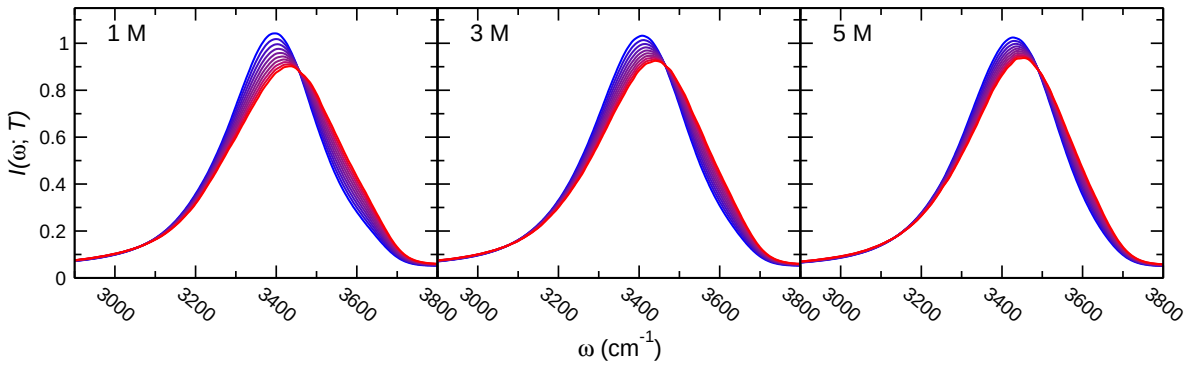

FIG. 10: Predicted IR spectrum for 280 K (blue) to 370 K (red) as a gradient in 10 K increments for NaCl in HOD/D_2O at 1 M (left), 3 M (middle), and 5 M (right).

isotopically dilute water. The aim is an investigation of how ions manifest their structure-making and breaking characteristics, implicit in the Hofmeister series ranking, in the vibrational spectroscopy. To this end, we have used fluctuation theory for dynamics to determine, from simulations at a single temperature, the temperature dependence of the IR spectrum and its contributions from the different interactions and motions present. These data provide insight into the driving forces for spectral changes with temperature, salt concentration, and salt identity.

The simulated IR spectra are in good agreement with previously reported measurements,[14,16,18,20,21] and are consistent with the Hofmeister series ranking of the halides. Specifically, the spectrum red-shifts with addition of KF, indicative of the stronger H-bonding expected of a "structure-maker," and blue-shifts as the other sodium-halide salts are added, characteristic of "structure-breaking" anions that disrupt the water H-bonding. The magnitude of this blue-shift increases with the size of the halide ion from chloride to iodide, as expected from the Hofmeister series.

The present results are based on the SPC/E water model and the Joung-Cheatham force field for the ions. This description is known to correctly describe the qualitative trends with ion identity and concentration of many dynamical properties for the systems considered here.[11,12,66,67] It will be interesting to investigate whether the effects observed here are also found in other fixed-charge classical force fields, *e.g.*, those derived from a Kirkwood-Buff analysis[68–70] or based on charge scaling,[71–76] and such work is currently underway in our lab. However, it is also known that polarizability and charge transfer effects, which are included only implicitly in fixed-charge descriptions, are important in water and electrolyte solutions. Such descriptions are also amenable to the fluctuation theory for dynamics approach used here and may provide new perspectives about the physical origins of changes in the water dynamics and spectroscopy with the addition of salts. We note that a recent exploration of several fixed charge and three-body water force fields found they all demonstrate the same mechanistic features for neat water diffusion, reorientation, and H-bond exchange.[61]

The origins of these changes are the main focus of the the present work and a key result is that they can be attributed almost exclusively to entropic effects. Namely, the calculated temperature derivative from fluctuation theory was used to determine effective internal energy and entropy profiles as a function of frequency that underlie the IR spectrum. The results show that the internal energy profile, while it changes with salt concentration, is only weakly dependent on the identity of the salt and particularly so for NaCl, NaBr, and NaI. On the other hand, the entropy changes significantly with the halide, reducing the entropic penalty to form stronger, more red-shifted H-bonds. This increase in the entropic favorability of strong H-bonds decreases with the size of the halide, consistent with the Hofmeister rankings. A secondary, but important effect for quantitative description of the spectra, is that the internal energy profile becomes less strongly dependent on frequency with increasing salt concentration, which makes the entropic effects more prominent in more concentrated solutions.

These results provide an interesting contrast with prior studies exploring the effect of ions on OH reorientation dynamics in water, which are directly linked to the exchange of H-bond acceptors by the OH group.[77,78] Stirnemann, Laage, Hynes, and co-workers have shown that the H-bond exchange time in the solvation shell of anions, relative to that in bulk water, can be understood as a product of two factors: 1) A slowdown related to the volume excluded by the anions that prevents the approach of potential new H-bond acceptors, and 2) A slowdown or acceleration associated with the strength of the water-anion H-bond compared to that of a water-water H-bond.[31,73,79–81] The first factor is fundamentally an entropic one and is consistent with the behavior observed here for the IR spectral changes in different salt solutions that depend on the size (excluded volume) of the anion. However, the second factor is not present to a significant degree in the IR spectra in contrast to the OH reorienta-

tion and H-bond exchange timescales. This difference is deserving of further study.

Finally, we used fluctuation theory to decompose the temperature derivative of the IR spectrum into contributions from different interactions present, both electrostatic and Lennard-Jones. The largest component is found to be water–water interactions that, however, decrease in magnitude as salt is added to the solution. Both water–ion and ion–ion electrostatic interactions contribute to the derivative with the former favoring more red-shifted frequencies corresponding to stronger H-bonding and the latter acting in opposition. The net result of the cancellation of these effects is comparatively small, but is important in determining how the temperature derivative changes with both salt concentration and identity. By extension, it also influences the effective internal energy of the spectrum as a function of frequency that we have used to predict the IR spectra as a function of temperature, consistent with experimental measurements.

SUPPORTING INFORMATION

Force field and empirical map parameters, simulation details, comparisons of KF and NaF results, comparison of frequency shifts to measured values, kinetic energy contributions to the IR spectra derivatives, and additional details of spectral features.

ACKNOWLEDGMENTS

The authors thank Profs. Damien Laage, Guillaume Stirnemann, and Andrei Tokmakoff for helpful comments. Dr. Zeke A. Piskulich is gratefully acknowledged for many useful discussions in the genesis of this research. This work was supported by the National Science Foundation under Grant No. CHE-2102656. A.K.B. gratefully acknowledges support from a University of Kansas Dean's Doctoral Fellowship. The calculations were performed at the University of Kansas Center for Research Computing (CRC).

[1]Harris, K. R.; Mills, R.; Back, P. J.; Webster, D. S. An improved NMR spin-echo apparatus for the measurement of self-diffusion coefficients: The diffusion of water in aqueous electrolyte solutions. *Biophys. J.* **1978**, *29*, 473–482.

[2]Collins, K. D.; Washabaugh, M. W. The Hofmeister effect and the behaviour of water at interfaces. *Q. Rev. Biophys.* **1985**, *18*, 323–422.

[3]Smith, J. D.; Saykally, R. J.; Geissler, P. L. The effects of dissolved halide anions on hydrogen bonding in liquid water. *J. Am. Chem. Soc.* **2007**, *129*, 13847–13856.

[4]Ohtaki, H.; Radnai, T. Structure and dynamics of hydrated ions. *Chem. Rev.* **1993**, *93*, 1157–1204.

[5]Bakker, H. J. Structural dynamics of aqueous salt solutions. *Chem. Rev.* **2008**, *108*, 1456–1473.

[6]Marcus, Y. Effect of ions on the structure of water: Structure making and breaking. *Chem. Rev.* **2009**, *109*, 1346–1370.

[7]Okazaki, Y.; Taniuchi, T.; Mogami, G.; Matubayasi, N.; Suzuki, M. Comparative study on the properties of hydration water of Na- and K-halide ions by Raman OH/OD-stretching spectroscopy and dielectric relaxation data. *J. Phys. Chem. A* **2014**, *118*, 2922–2930.

[8]Xie, W. J.; Gao, Y. Q. A simple theory for the Hofmeister series. *J. Phys. Chem. Lett.* **2013**, *4*, 4247–4252.

[9]Assaf, K. I.; Nau, W. M. The chaotropic effect as an assembly motif in chemistry. *Angew. Chem. Int. Ed.* **2018**, *57*, 13968–13981.

[10]Zangi, R. Can salting-in/salting-out ions be classified as chaotropes/kosmotropes? *J. Phys. Chem. B* **2010**, *114*, 643–650.

[11]Kim, J. S.; Wu, Z.; Morrow, A. R.; Yethiraj, A.; Yethiraj, A. Self-diffusion and viscosity in electrolyte solutions. *J. Phys. Chem. B* **2012**, *116*, 12007–12013.

[12]Borkowski, A. K.; Piskulich, Z. A.; Thompson, W. H. Examining the Hofmeister series through activation energies: Water diffusion in aqueous alkali-halide solutions. *J. Chem. Phys. B* **2021**, *125*, 350–359.

[13]Freire, M. G.; Neves, C. M.; Silva, A. M.; Santos, L. M.; Marrucho, I. M.; Rebelo, L. P.; Shah, J. K.; Maginn, E. J.; Coutinho, J. A. ^{1}H NMR and molecular dynamics evidence for an unexpected interaction on the origin of salting-in/salting-out phenomena. *J. Phys. Chem. B* **2010**, *114*, 2004–2014.

[14]Waldron, R. D. Infrared spectra of HDO in water and ionic solutions. *J. Chem. Phys.* **1957**, *26*, 809–814.

[15]Busing, W. R.; Hornig, D. F. The effect of dissolved KBr, KOH, or HCl on the Raman spectrum of water. *J. Phys. Chem.* **1961**, *65*, 284–292.

[16]Hartman, K. A. The structure of water and the stability of the secondary structure in biological molecules. An infrared and proton magnetic resonance study. *J. Phys. Chem.* **1966**, *70*, 270–276.

[17]Wall, T. T.; Hornig, D. F. Raman spectra of water in concentrated ionic solutions. *J. Chem. Phys.* **1967**, *47*, 784–792.

[18]Wyss, H. R.; Falk, M. Infrared spectrum of HDO in water and in NaCl solution. *Can. J. Chem.* **1970**, *48*, 607–614.

[19]Terpstra, P.; Combes, D.; Zwick, A. Effect of salts on dynamics of water: A Raman spectroscopy study. *J. Chem. Phys.* **1990**, *92*, 65–70.

[20]Masuda, K.; Haramaki, T.; Nakashima, S.; Habert, B.; Martinez, I.; Kashiwabara, S. Structural change of water with solutes and temperature up to 100 °C in aqueous solutions as revealed by attenuated total reflectance infrared spectroscopy. *Appl. Spectrosc* **2003**, *57*, 274–281.

[21]Kropman, M. F.; Bakker, H. J. Vibrational relaxation of liquid water in ionic solvation shells. *Chem. Phys. Lett.* **2003**, *370*, 741–746.

[22]Kropman, M. F.; Bakker, H. J. Effect of ions on the structure and dynamics of liquid water. *J. Phys.: Condens. Matter* **2005**, *17*, S3215–S3224.

[23]Nickolov, Z. S.; Miller, J. D. Water structure in aqueous solutions of alkali halide salts: FTIR spectroscopy of the OD stretching band. *J. Colloid Interface Sci.* **2005**, *287*, 572–580.

[24]Max, J.-J.; Gessinger, V.; van Driessche, C. Infrared spectroscopy of aqueous ionic salt solutions at low concentrations. *J. Chem. Phys.* **2007**, *126*, 184507.

[25]Perera, P. N.; Browder, B.; Ben-Amotz, D. Perturbations of water by alkali halide ions measured using multivariate Raman curve resolution. *J. Phys. Chem. B* **2009**, *113*, 1805–1809.

[26]Moilanen, D. E.; Wong, D. B.; Rosenfeld, D. E.; Fenn, E. E.; Fayer, M. D. Ion-Water hydrogen-bond switching observed with 2D IR vibrational echo chemical exchange spectroscopy. *Proc. Natl. Acad. Sci. USA* **2009**, *106*, 375–380.

[27]Tielrooij, K. J.; Garcia-Araez, N.; Bonn, M.; Bakker, H. J. Cooperativity in ion hydration. *Science* **2010**, *328*, 1006–1009.

[28]Post, S. T. D.; Bakker, H. J. The combined effect of cations and anions on the dynamics of water. *Phys. Chem. Chem. Phys.* **2012**, *14*, 6280–6288.

[29]Giammanco, C. H.; Wong, D. B.; Fayer, M. D. Water dynamics in divalent and monovalent concentrated salt solutions. *J. Phys. Chem. B* **2012**, *116*, 13781–13792.

[30]Okur, H. I.; Hladílková, J.; Rembert, K. B.; Cho, Y.; Heyda, J.; Dzubiella, J.; Cremer, P. S.; Jungwirth, P. Beyond the Hofmeister series: Ion-specific effects on proteins and their biological functions. *J. Phys. Chem. B* **2017**, *121*, 1997–2014.

[31]Stirnemann, G.; Wernersson, E.; Jungwirth, P.; Laage, D. Mechanisms of acceleration and retardation of water dynamics by ions. *J. Am. Chem. Soc.* **2013**, *135*, 11824–11831.

[32]Xie, W. J.; Yang, Y. I.; Gao, Y. Q. Dual reorientation relaxation routes of water molecules in oxyanion's hydration shell: A molecular geometry perspective. *J. Chem. Phys.* **2015**, *143*, 224504.

[33]Gaiduk, A. P.; Galli, G. Local and global effects of dissolved sodium chloride on the structure of water. *J. Phys. Chem. Lett.* **2017**, *8*, 1496–1502.

[34]Oncsik, T.; Trefalt, G.; Borkovec, M.; Szilagyi, I. Specific ion effects on particle aggregation induced by monovalent salts within the Hofmeister series. *Langmuir* **2015**, *31*, 3799–3807.

[35]Walrafen, G. E. Raman spectral studies of the effects of solutes and pressure on water structure. *J. Chem. Phys.* **1971**, *55*, 768–792.

[36]Corcelli, S. A.; Lawrence, C. P.; Skinner, J. L. Combined electronic structure/molecular dynamics approach for ultrafast infrared spectroscopy of dilute HOD in liquid H_2O and D_2O. *J. Chem. Phys.* **2004**, *120*, 8107–8117.

[37]Auer, B.; Kumar, R.; Schmidt, J. R.; Skinner, J. L. Hydrogen bonding and Raman, IR, and 2D-IR spectroscopy of dilute HOD in liquid D_2O. *Proc. Natl. Acad. Sci.* **2007**, *104*, 14215–14220.

[38]Hare, D. E.; Sorensen, C. M. Interoscillator coupling effects on the OH stretching band of liquid water. *J. Chem. Phys.* **1992**, *96*, 13–22.

[39]Torii, H. Time-domain calculations of the polarized Raman spectra, the transient infrared absorption anisotropy, and the extent of delocalization of the OH stretching mode of liquid water. *J. Phys. Chem. A* **2006**, *110*, 9469–9477.

[40]Schmidt, J. R.; Corcelli, S. A.; Skinner, J. L. Pronounced non-Condon effects in the ultrafast infrared spectroscopy of water. *J. Chem. Phys.* **2005**, *123*, 044513.

[41]Corcelli, S. A.; Skinner, J. L. Infrared and Raman line shapes of dilute HOD in liquid H_2O and D_2O from 10 to 90°C. *J. Phys. Chem. A* **2005**, *109*, 6154–6165.

[42]Lin, Y.-S.; Auer, B. M.; Skinner, J. L. Water structure, dynamics, and vibrational spectroscopy in sodium bromide solutions. *J. Chem. Phys.* **2009**, *131*, 144511.

[43]Gruenbaum, S. M.; Tainter, C. J.; Shi, L.; Skinner, J. L. Robustness of frequency, transition dipole, and coupling maps for water vibrational spectroscopy. *J. Chem. Theory Comput.* **2013**, *9*, 3109–3117.

[44]Mesele, O. O.; Thompson, W. H. Removing the barrier to the calculation of activation energies. *J. Chem. Phys.* **2016**, *145*, 134107.

[45]Piskulich, Z. A.; Mesele, O. O.; Thompson, W. H. Activation energies and beyond. *J. Phys. Chem. A* **2019**, *123*, 7185–7194.

[46]Piskulich, Z. A.; Thompson, W. Temperature dependence of the water infrared spectrum: Driving forces, isosbestic points, and predictions. *J. Phys. Chem. Lett.* **2020**, *11*, 7762–7768.

[47]Fecko, C. J.; Loparo, J. J.; Roberts, S. T.; Tokmakoff, A. Local hydrogen bonding dynamics and collective reorganization in water: Ultrafast infrared spectroscopy of HOD/D_2O. *J. Chem. Phys.* **2005**, *122*, 054506.

[48]Greene, R. F.; Callen, H. B. On the formalism of thermodynamic fluctuation theory. *Phys. Rev.* **1951**, *83*, 1231–1235.

[49]Hill, T. L. *Statistical Mechanics. Principles and Selected Applications*; Dover: New York, 1956.

[50]The LAMMPS molecular dynamics package, http://lammps.sandia.gov (downloaded July 8, 2020).

[51]Plimpton, S. Fast parallel algorithms for short-range molecular dynamics. *J. Comput. Phys.* **1995**, *117*, 1–19.

[52]Berendsen, H. J. C.; Grigera, J. R.; Straatsma, T. P. The missing term in effective pair potentials. *J. Phys. Chem.* **1987**, *91*, 6269–6271.

[53]Joung, I. S.; Cheatham III, T. E. Determination of alkali and halide monovalent ion parameters for use in explicitly solvated biomolecular simulations. *J. Phys. Chem. B* **2008**, *112*, 9020–9041.

[54]Reynolds, J. G.; Belsher, J. D. A review of sodium fluoride solubility in water. *J. Chem. Eng. Data* **2017**, *62*, 1743–1748.

[55]Shoemaker, D. P.; Garland, C. W.; Nibler, J. W. *Experiments in Physical Chemistry*; McGraw-Hill: New York, 1989.

[56]Geissler, P. L. Temperature dependence of inhomogeneous broadening: On the meaning of isosbestic points. *J. Am. Chem. Soc.* **2005**, *127*, 14930–14935.

[57]Hare, D. E.; Sorensen, C. M. Raman spectroscopic study of dilute HOD in liquid H_2O in the temperature range −31.5 to 160°C. *J. Chem. Phys.* **1990**, *93*, 6954–6961.

[58]Walrafen, G. E. Effects of equilibrium H-bond distance and angle changes on Raman intensities from water. *J. Chem. Phys.* **2004**, *120*, 4868–4876.

[59]Piskulich, Z. A.; Mesele, O. O.; Thompson, W. H. Removing the barrier to the calculation of activation energies: Diffusion coefficients and reorientation times in liquid water. *J. Chem. Phys.* **2017**, *147*, 134103.

[60]Piskulich, Z. A.; Thompson, W. H. The dynamics of supercooled water can be predicted from room temperature simulations. *J. Chem. Phys.* **2020**, *152*, 074505.

[61]Piskulich, Z. A.; Thompson, W. H. Examining the role of different molecular interactions on activation energies and activation volumes in liquid water. *J. Chem. Theory Comput.* **2021**, *17*, 2659–2671.

[62]Piskulich, Z. A.; Thompson, W. H. The activation energy for water reorientation differs between IR pump-probe and NMR measurements. *J. Chem. Phys.* **2018**, *149*, 164504.

[63]Piskulich, Z. A.; Laage, D.; Thompson, W. H. Activation energies and the extended jump model: How temperature affects reorientation and hydrogen-bond exchange dynamics in water. *J. Chem. Phys.* **2020**, *153*, 074110.

[64]Mendis, C. H.; Piskulich, Z. A.; Thompson, W. H. Tests of the Stokes-Einstein relation through the shear viscosity activation energy of water. *J. Phys. Chem. B* **2019**, *123*, 5857–5865.

[65]Abascal, J. L.; Vega, C. A general purpose model for the condensed phases of water: TIP4P/2005. *J. Chem. Phys.* **2005**, *123*, 234505.

[66]Joung, I. S.; Cheatham III, T. E. Molecular Dynamics Simulations of the Dynamic and Energetic Properties of Alkali and Halide Ions Using Water-Model-Specific Ion Parameters. *J. Phys. Chem. B* **2009**, *113*, 13279–13290.

[67]Döpke, M. F.; Moultos, O. A.; Hartkamp, R. On the transferability of ion parameters to the TIP4P/2005 water model using molecular dynamics simulations. *J. Chem. Phys.* **2020**, *152*, 024501.

[68]Gee, M. B.; Cox, N. R.; Jiao, Y.; Bentenitis, N.; Weerasinghe, S.; Smith, P. E. A Kirkwood-Buff derived force field for aqueous alkali halides. *J. Chem. Theory Comput.* **2011**, *7*, 1369–1380.

[69]Fyta, M.; Netz, R. R. Ionic force field optimization based on single-ion and ion-pair solvation properties: Going beyond standard mixing rules. *J. Chem. Phys.* **2012**, *136*.

[70]Loche, P.; Steinbrunner, P.; Friedowitz, S.; Netz, R. R.; Bonthuis, D. J. Transferable ion force fields in water from a simultaneous optimization of ion solvation and ion-ion interaction. *J. Phys. Chem. B* **2021**, *125*, 8581–8587.

[71]Kohagen, M.; Mason, P. E.; Jungwirth, P. Accounting for electronic polarization effects in aqueous sodium chloride via molecular dynamics aided by neutron scattering. *J. Phys. Chem. B* **2016**, *120*, 1454–1460.

[72]Kirby, B. J.; Jungwirth, P. Charge scaling manifesto: A way of reconciling the inherently macroscopic and microscopic natures of molecular simulations. *J. Phys. Chem. Lett.* **2019**, *10*, 7531–7536.

[73]Laage, D.; Stirnemann, G. Effect of ions on water dynamics in dilute and concentrated aqueous salt solutions. *J. Phys. Chem. B* **2019**, *123*, 3312–3324.
[74]Benavides, A. L.; Portillo, M. A.; Chamorro, V. C.; Espinosa, J. R.; Abascal, J. L. F.; Vega, C. A potential model for sodium chloride solutions based on the TIP4P/2005 water model. *J. Chem. Phys.* **2017**, *147*, 104501.
[75]Zeron, I. M.; Abascal, J. L. F.; Vega, C. A force field of Li^+, Na^+, K^+, Mg^{2+}, Ca^{2+}, Cl^-, and SO_4^{2-} in aqueous solution based on the TIP4P/2005 water model and scaled charges for the ions. *J. Chem. Phys.* **2019**, *151*, 134504.
[76]Blazquez, S.; Conde, M.; Abascal, J. L. F.; Vega, C. The Madrid-2019 force field for electrolytes in water using TIP4P/2005 and scaled charges: Extension to the ions F^-, Br^-, I^-, Rb^+, and Cs^+. *J. Chem. Phys.* **2022**, *156*, 044505.
[77]Laage, D.; Hynes, J. T. A molecular jump mechanism of water reorientation. *Science* **2006**, *311*, 832–835.
[78]Laage, D.; Hynes, J. T. On the molecular mechanism of water reorientation. *J. Phys. Chem. B* **2008**, *112*, 14230–14242.
[79]Laage, D.; Stirnemann, G.; Sterpone, F.; Rey, R.; Hynes, J. T. Reorientation and allied dynamics in water and aqueous solutions. *Annu. Rev. Phys. Chem.* **2011**, *62*, 395–416.
[80]Boisson, J.; Stirnemann, G.; Laage, D.; Hynes, J. T. Water reorientation dynamics in the first hydration shells of F^- and I^-. *Phys Chem Chem Phys* **2011**, *13*, 19895.
[81]Stirnemann, G.; Jungwirth, P.; Laage, D. Water dynamics in concentrated electrolytes: Local ion effect on hydrogen-bond jumps rather than collective coupling to ion clusters. *Proc. Natl. Acad. Sci. USA* **2018**, *115*, E4953–E4954.

TOC Graphic